JBC RESEARCH ARTICLE

An examination of the metal ion content in the active sites of human endonucleases CPSF73 and INTS11

Received for publication, January 19, 2023, and in revised form, February 13, 2023 Published, Papers in Press, February 22, 2023,
https://doi.org/10.1016/j.jbc.2023.103047

Ji Huang[1,‡], **Xiangyang Liu**[1,‡], **Yadong Sun**[1,‡], **Zhuang Li**[1], **Min-Han Lin**[1], **Keith Hamilton**[1], **Corey R. Mandel**[1], **Felix Sandmeir**[2], **Elena Conti**[2], **Paul H. Oyala**[3], **and Liang Tong**[1,*]

From the [1]*Department of Biological Sciences, Columbia University, New York, New York, USA;* [2]*Department of Structural Cell Biology, Max Planck Institute of Biochemistry, Martinsried, Germany;* [3]*Division of Chemistry and Chemical Engineering, California Institute of Technology, Pasadena, California, USA*

Reviewed by members of the JBC Editorial Board. Edited by Karin Musier-Forsyth

Human cleavage and polyadenylation specificity factor (CPSF)73 (also known as CPSF3) is the endoribonuclease that catalyzes the cleavage reaction for the 3′-end processing of pre-mRNAs. The active site of CPSF73 is located at the interface between a metallo-β-lactamase domain and a β-CASP domain. Two metal ions are coordinated by conserved residues, five His and two Asp, in the active site, and they are critical for the nuclease reaction. The metal ions have long been thought to be zinc ions, but their exact identity has not been examined. Here we present evidence from inductively coupled plasma mass spectrometry and X-ray diffraction analyses that a mixture of metal ions, including Fe, Zn, and Mn, is present in the active site of CPSF73. The abundance of the various metal ions is different in samples prepared from different expression hosts. Zinc is present at less than 20% abundance in a sample expressed in insect cells, but the sample is active in cleaving a pre-mRNA substrate in a reconstituted canonical 3′-end processing machinery. Zinc is present at 75% abundance in a sample expressed in human cells, which has comparable endonuclease activity. We also observe a mixture of metal ions in the active site of the CPSF73 homolog INTS11, the endonuclease for Integrator. Taken together, our results provide further insights into the role of metal ions in the activity of CPSF73 and INTS11 for RNA 3′-end processing.

Eukaryotic pre-mRNAs need to undergo 3′-end processing during their maturation. The majority of pre-mRNAs are cleaved and polyadenylated at the 3′-end, which involves an endonucleolytic cleavage followed by the addition of a polyadenylate (poly(A)) tail (1–5). A large machinery with many protein factors is required for this canonical 3′-end processing. In comparison, replication-dependent histone pre-mRNAs in animals are cleaved but not polyadenylated at the 3′-end, and a distinct machinery, the U7 snRNP, is required for this processing (6).

Cleavage and polyadenylation specificity factor (CPSF)73 (also known as CPSF3) is the endonuclease for the cleavage reaction in both machineries (7–9). In the canonical machinery, CPSF73 is a part of the mammalian cleavage factor (mCF) (10, 11), which also contains CPSF100 and symplekin. mCF and mammalian polyadenylation specificity factor (mPSF, with CPSF160, WDR33, CPSF30, and Fip1) are the two components of the CPSF. Cleavage stimulation factor (CstF, with CstF50, CstF64, and CstF77), cleavage factor Im (CFIm, with CFIm25 and CFIm68 or CFIm59), CFIIm (with Clp1 and Pcf11), poly(A) polymerase (PAP), and RBBP6 (12–14) have also been identified for this machinery. In the U7 snRNP, CPSF73 is a part of the histone pre-mRNA cleavage complex (HCC) (15), which also contains CPSF100, symplekin, and CstF64. Therefore, mCF and HCC are equivalent to each other, with the difference being the presence of CstF64 in HCC. This CstF64 in HCC is not required for histone pre-mRNA 3′-end processing, and its function is not known.

CPSF73 belongs to the metallo-β-lactamase family of enzymes (16, 17), and its catalytic segment (residues 1–460) contains a metallo-β-lactamase domain and a β-CASP domain (9) (Fig. 1*A*). The active site is located at the interface between the two domains. Two transition metal ions are coordinated by a collection of five His and two Asp residues in the active site (Fig. 1*B*). The structure of a reconstituted, active U7 snRNP bound to a pre-mRNA substrate shows that the two metal ions are critical for catalysis, coordinating the scissile phosphate of the pre-mRNA and activating the water/hydroxide that initiates the nucleophilic attack on the phosphorus atom in the scissile phosphate for the nuclease reaction (18) (Fig. 1*B*). A sulfate ion observed in the crystal structure of CPSF73 catalytic segment (9) (Fig. 1*B*) is a mimic of the scissile phosphate. Mutation of a residue coordinating the metal ion in the active site of CPSF73 abolished the cleavage activity.

Human INTS11 is a homolog of CPSF73 and is the endonuclease for the cleavage reaction of Integrator, a multisubunit machinery that is required for snRNA 3′-end processing and mRNA transcription attenuation (19–22).

‡ Equal first authors.
* For correspondence: Liang Tong, ltong@columbia.edu.
Present addresses for: Yadong Sun, School of Life Science and Technology, ShanghaiTech University, Shanghai, China; Keith Hamilton, Rockefeller University, New York, NY 10065; Zhuang Li, School of Life Sciences, Hubei University, Wuhan, China; Corey R. Mandel, Genentech, Inc, South San Francisco, CA 94080.

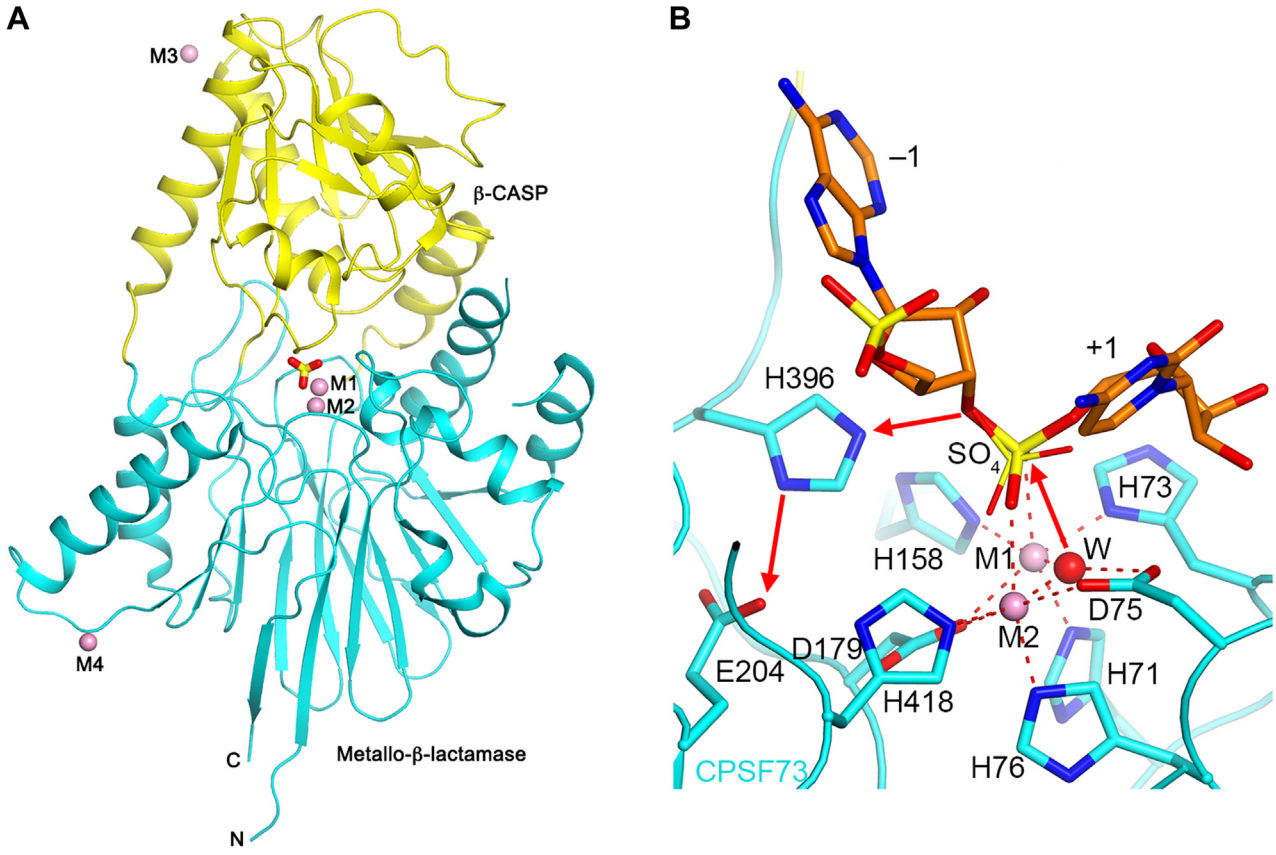

Figure 1. Structure and the active site of CPSF73. *A,* overall structure of the human CPSF73 catalytic segment with four metal ions. The metallo-β-lactamase and β-CASP domains are shown in *cyan* and *yellow*, respectively (PDB entry 2I7V) (9). The metal ions are shown as *pink spheres* and labeled. A sulfate ion coordinated to the metal ions in the active site is shown in *sticks*. *B,* coordination of the two metal ions in the active site of CPSF73. The sulfate ion is shown as *thin sticks*. The bound positions of the nucleotides in the pre-mRNA substrate just before (−1) and after (+1) the cleavage site are also shown (18). The cleavage is initiated by the bridging hydroxide attacking the scissile phosphate, and the leaving group is stabilized by conserved His396, which in turn interacts with conserved Glu204 (*red arrows*). Produced with PyMOL (www.pymol.org). CPSF, cleavage and polyadenylation specificity factor.

INTS11 is a part of the integrator cleavage module (ICM), which also contains INTS9 and INTS4, with INTS9 being a homolog of CPSF100.

The two metal ions in the active site of CPSF73 have long been thought to be zinc ions. However, metallo-β-lactamases can also use other divalent transition metal ions for catalysis, such as Mn and Fe (23–25). To the best of our knowledge, the exact identity of the metal ions in CPSF73 has not been examined. Here we used inductively coupled plasma mass spectrometry (ICP-MS) and X-ray diffraction analyses to show that a mixture of metal ions is present in the active site of CPSF73 and INTS11. A sample of mCF expressed in insect cells has ∼65% iron and only 18% zinc in the CPSF73 active site, but it is active in cleaving a model pre-mRNA substrate in a reconstituted canonical 3′-end processing machinery. A sample of HCC expressed in human cells has ∼75% zinc and 24% iron in the CPSF73 active site, which has comparable endonuclease activity. Electron paramagnetic resonance (EPR) spectroscopy of a sample of the CPSF73 catalytic segment expressed in bacteria indicates the presence of both Fe(III) and Fe(II) oxidation states through detection of a high spin S = 5/2 Fe(III) species, as well as an S = ½ species consistent with an antiferromagnetically coupled Fe(II)-Fe(III) diiron center.

Results

Zinc absorption peak was not detected for crystals of the catalytic segment of CPSF73

We determined the crystal structure of the catalytic segment of human CPSF73 (residues 1–460) earlier by zinc anomalous signal, using a crystal grown in the presence of 0.3 mM $ZnCl_2$ (9). X-ray diffraction data were collected at the Zn absorption peak (1.283 Å), and four metal ions were located based on the anomalous signal. Two of the metal ions are located in the active site of CPSF73 (M1, M2), and the other two are on the surface (M3, M4) (Fig. 1*A*).

However, while crystals grown in the presence of $ZnCl_2$ gave clear X-ray absorption signals when they were scanned near the Zn absorption edge, crystals grown without extra Zn showed no such signal, even though electron density for two metal ions was observed in the active site based on the X-ray diffraction data. At the time, it was thought that this lack of an absorption signal was due to the low abundance of two Zn ions

relative to a protein of 460 amino acid residues in the crystal, and all four sites were interpreted as zinc.

Predominantly iron in the sample of CPSF73 catalytic segment

To obtain an independent assessment of the identities of the metal ions in the active site of CPSF73, we subjected the purified sample of human CPSF73 catalytic segment to ICP-MS analysis. This was carried out in 2007, with the same protein sample that was used to grow the crystals for the structure determination (9). The abundance of all first-row transition metal ions was examined, V, Cr, Mn, Fe, Co, Ni, Cu, and Zn. The results showed that iron had the highest abundance, at ∼81%, while Cr and Co were below their limits of detection (Table 1). The abundance of Zn was only ∼3%, which would explain why crystals of this sample failed to show an X-ray absorption peak for Zn. Mn was the second most abundant metal ion, at ∼13%.

The ICP-MS and crystallographic data suggest that the two metal ions in the active site of CPSF73 catalytic segment (M1 and M2, Fig. 1) are predominantly iron. The two metal ions on the surface (M3 and M4) are most likely zinc ions, from the 0.3 mM $ZnCl_2$ in the crystallization solution. This also demonstrates that the zinc ions in the crystallization solution are not able to replace the metal ions that are already bound in the active site of CPSF73.

The crystal grown in the presence of 0.3 mM $ZnCl_2$ diffracted to 2.1 Å resolution (PDB entry 2I7V) (9). The anomalous difference electron-density map, calculated using reflections between 15 and 3 Å resolution in the dataset collected at the Zn peak, showed four peaks (Table 2). The two metal ions in the active site (M1 and M2) have peak heights of 22.2 and 26.7 σ, as iron and manganese both have appreciable anomalous signals at the zinc absorption peak (Table 2). The metal ion with the highest peak (37.3 σ) is one of those on the surface (M3), which gives an indication for the anomalous signal expected from a genuine zinc ion in this experiment. The metal ion M3 is located at a crystal packing interface, and its binding is likely stabilized by these interactions. It has a temperature factor of 50 $Å^2$, comparable to those of protein atoms in this region. The metal ion M4 is also located on the surface but is not involved in crystal packing, and it has a high temperature factor value (99 $Å^2$), consistent with its lower peak height (Table 2).

The sample of human CPSF73 catalytic segment was prepared from *Escherichia coli* expression, and the activity of this sample was very low (9). Therefore, it was not clear whether having iron in the active site of CPSF73 can support its nuclease activity, and the presence of iron in this sample could also be a consequence of the expression in bacteria. It is necessary to analyze the metal ion content of a sample that is active for RNA cleavage.

RNA cleavage activity with the canonical machinery

We succeeded in reconstituting an active U7 snRNP, using all recombinant human proteins expressed in insect cells or *E. coli*, which showed good cleavage activity toward a model histone pre-mRNA substrate (18, 26, 27). The structure of this machinery bound to a pre-mRNA revealed how CPSF73 assumes an open conformation to bind the RNA for the cleavage reaction and how the two metal ions in the active site are critical for the catalysis (18).

For the canonical machinery, we observed cleavage activity with a HeLa cell nuclear extract, using a 70-mer RNA substrate encompassing the SV40 late mRNA 3′-end processing site. We found that this nuclear extract on its own had very low cleavage activity, and supplementing with recombinant human CFIIm increased the activity (Fig. 2*A*), and additional supplementation with PAP resulted in greatly enhanced activity (Fig. 2*B*). Higher concentrations of CFIIm are better for the cleavage activity (Fig. 2*A*), and the Pcf11 FEGP repeats (28) are required for the increased activity (Fig. 2*C*). We also found that the 3′-dATP that is typically included in 3′-end processing assays can be replaced with ATP, ADP, or ATPγS in our experiments while AMP is much less active (Fig. 2, *D* and *E*), and other nucleotides GTP, CTP, and UTP cannot support the cleavage reaction (Fig. 2*E*). The optimal concentration of the nucleotide is ∼2 mM. ATP can be used probably because PAP is not active under this assay condition due to the lack of Mg^{2+} ions and the presence of EDTA in the reaction buffer. Polyethylene glycol (PEG) is required while creatine phosphate is dispensable under our assay conditions (Fig. 2*F*). A time course of the cleavage reaction in the presence of nuclear extract, 0.5 μM CFIIm, and 0.5 μM PAP indicated that more than 80% of the substrate was cleaved in 2 h (Fig. 2, *G* and *H*).

We also succeeded in reconstituting an active canonical machinery using all recombinant proteins expressed in insect cells, based on the published identification of the essential role of RBBP6 (13, 14). Using purified human mPSF, mCF (or HCC), CstF, CFIIm, RBBP6 (1–399), and PAP (D115A active

Table 1
Metal ion abundance in human CPSF73 and INTS11 by ICP-MS

Metal ion abundance (%)	CPSF73 catalytic segment expressed in bacteria	Human mCF expressed in insect cells	Human HCC expressed in human cells	Human ICM expressed in insect cells
V	0.02	n. e.	n. e.	n. e.
Cr	<LOD	n. e.	n. e.	n. e.
Mn	12.8	11.3	1.3	41.1
Fe	81.1	65.3	23.5	31.2
Co	<LOD	n. e.	n. e.	n. e.
Ni	2.2	5.5	0.3	1.6
Cu	0.84	n. e.	n. e.	n. e.
Zn	3.1	17.8	74.8	26.1

Abbreviations: LOD, limit of detection; n.e., not examined.

Table 2
Peak heights in anomalous difference electron density maps

	Crystal grown in the presence of 0.3 mM $ZnCl_2$	Crystal grown without additional zinc		
Wavelength (Å)	1.283 (Zn peak)	1.283 (Zn peak)	1.738 (Fe peak)	1.892 (Mn peak)
Dataset resolution (Å)	2.1	2.3	2.3	2.3
Zn anomalous signal (Δf′)	3.9	3.9	0.8	1.0
Fe anomalous signal (Δf′)	2.4	2.4	4.0	0.5
Mn anomalous signal (Δf′)	2.0	2.0	3.3	4.0
Data resolution for map (Å)	15–3	15–3	15–3	15–3
Peak heights (σ)				
M1	22.2	16.8	24.7	9.2
M2	26.7	23.9	28.4	14.1
M3	37.3	–	–	–
M4	17.1	–	–	–

site mutant), we observed good cleavage activity with the 70-mer RNA substrate (Fig. 3*A*). Nearly 50% of the RNA substrate was cleaved after a 2 h incubation under the condition tested (Fig. 3*B*). Roughly 20% of the substrate was cleaved in the first 20 min. Then, the reaction slowed down substantially, with 60 min needed to cleave the next 20% of the substrate. Mg^{2+} was included in the assay buffer for potentially helping with ATP binding, but it is not required for the cleavage activity (Fig. S1*A*). Overall, we have produced samples of HCC/mCF from baculovirus-infected insect cells that are active for RNA cleavage.

Substantial iron content in mCF/HCC with active human CPSF73

We next subjected a sample of the active human mCF expressed in insect cells to ICP-MS analysis and examined the four metal irons that showed good abundance in the catalytic segment, Fe, Mn, Zn, and Ni. Iron was again found to be the most abundant, at ∼65% (Table 1). The abundance of zinc was higher in this sample, ∼18%. Since the other proteins in mCF (CPSF100 and symplekin) are not known to bind metal ions (18), the ICP-MS analysis confirms that iron is the most abundant metal ion in the active site of CPSF73 in this active mCF sample expressed in insect cells.

We also examined by ICP-MS the metal ion content of an active human HCC sample expressed in human cells (13). Zinc was found to be the most abundant in this sample, at ∼75% (Table 1), but there was still a substantial amount of iron in this sample (24%). The cleavage activity of this sample is generally comparable to that of human mCF expressed in insect cells (Fig. S2), despite their different zinc content.

We assessed whether the inclusion of extra metal ions in the assay buffer could affect the cleavage activity. We tested various concentrations of $Zn(OAc)_2$, $Fe(II)SO_4$, and $Fe(III)Cl_3$ and observed essentially no change in the activity (Fig. S1, *B*–*D*). This is consistent with the hypothesis that CPSF73 is active with iron and/or zinc in the active site. This is also consistent with our observations during the structure determination of the catalytic segment of CPSF73, showing that metal ions are bound to the active site of CPSF73 during protein expression and are not exchangeable with metal ions in the buffers during purification and crystallization.

Crystallographic analysis supports the presence of iron in CPSF73 catalytic segment

With the ICP-MS results on active CPSF73, we carried out further crystallographic analysis on crystals of the catalytic segment of human CPSF73. We reproduced the crystals reported earlier (9), without any zinc in the crystallization solution, and collected good quality X-ray diffraction data to 2.3 Å resolution at the Zn, Fe, and Mn absorption peaks at beamline 24-ID-C at the Advanced Photon Source (Table S1). We then used data between 15 and 3 Å resolution to calculate anomalous difference electron density maps. Two strong peaks were observed in the dataset collected at the Zn peak, corresponding to the two metal ions in the active site (M1, M2), and these peaks are even stronger in the dataset collected at the Fe peak (Table 2). Importantly, zinc should have a very small anomalous signal at the Fe peak (0.8, Table 2), and therefore, the two stronger peaks in the anomalous difference map at the iron peak indicate that the two metal ions are mostly iron and not zinc, consistent with the ICP-MS analysis.

At the Mn peak, both Zn (1.0) and Fe (0.5) have small anomalous signals, and we observed weaker peaks for the two metal ions (Table 2), consistent with the lower abundance of Mn in the active site. In fact, at this longer wavelength, we observed many additional peaks that correspond to sulfur atoms in the side chains of Cys and Met residues in CPSF73 (for example Met424, 8.0σ; Cys153, 6.9σ; Met95, 6.4σ; Met166, 6.1σ), illustrating the quality of the diffraction data. The two metal ions outside the active site (M3, M4) were not observed in any of the three datasets (Table 2), consistent with them being from the 0.3 mM $ZnCl_2$ in the crystallization solution.

The anomalous difference electron density maps also indicate that Fe and Mn are present at both positions (M1 and M2) in the active site, while the distribution of Zn could not be clearly defined due to its low abundance. Overall, these additional X-ray diffraction analyses support the ICP-MS data, indicating the presence of metal ions other than zinc at both positions in the active site of CPSF73.

Oxidation states of iron in the CPSF73 catalytic segment

We next characterized the oxidation state of iron in the CPSF73 catalytic segment by EPR spectroscopy. Samples were prepared at an approximate concentration of 300 μM in the same buffer as that used for other assays, with the addition of

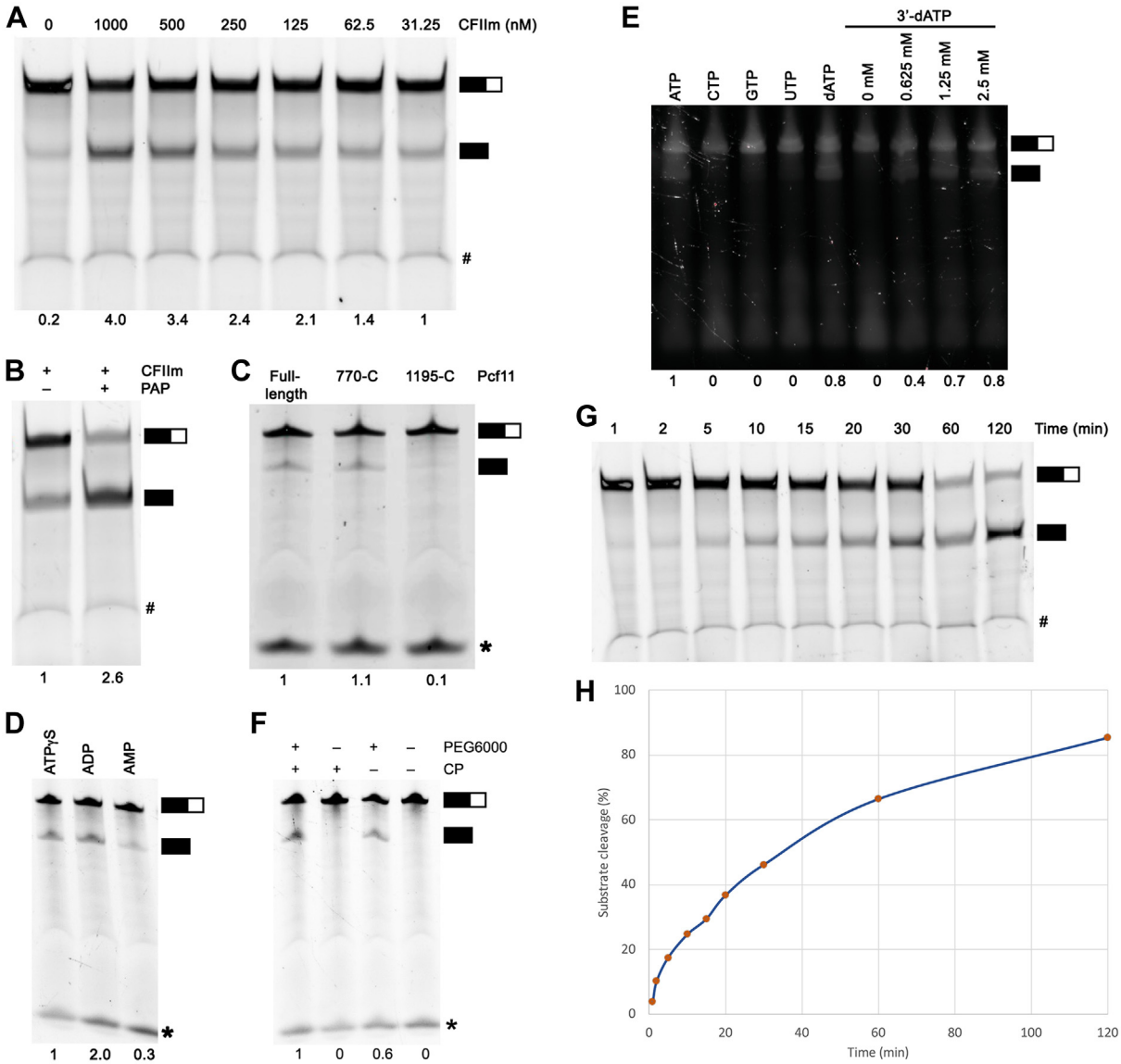

Figure 2. Characterization of the cleavage activity of a nuclear extract supplemented with purified recombinant protein factors. *A,* supplementation with human CFIIm (expressed in insect cells) increases the cleavage activity of a HeLa cell nuclear extract (from Ipracell). The 70-mer pre-mRNA substrate is indicated with the *black* and *white bar*, and the 45-mer 5′ cleavage product is indicated with the *black bar*. The 25-mer 3′ product is not visible. An artificial feature in the gel is indicated with #. The relative amounts of the cleavage product in the different lanes are indicated, estimated using ImageJ (56). Most of the experiments in this figure are carried out at least two times, with similar results. *B,* additional supplementation with PAP greatly enhanced the activity. *C,* full-length Pcf11 and a 770-C terminus construct, which contain the FEGP repeats, are active with the nuclear extract. The 1195-C construct, which lacks the FEGP repeats, shows very weak activity. The band at the *bottom* of the gel is due to nonspecific degradation of the RNA substrate by the nuclear extract, indicated with the *asterisk*. *D,* the effects of various adenine nucleotides on the cleavage activity. *E,* the effects of various nucleotides on the cleavage activity, and a concentration titration with 3′-dATP. *F,* the effects of PEG6000 and creatine phosphate (CP) on the cleavage activity. *G,* a time course of the cleavage reaction in the presence of nuclear extract, CFIIm, and PAP. Some of the sample for the 60 min time point was lost during handling, but it did not affect the percentage of substrate cleavage. *H,* the reaction time course converted to percentage of substrate cleavage, based on the intensity of the substrate and product bands. PAP, poly(A) polymerase.

10% (v/v) glycerol as a cryoprotectant. The X-band (9.6 GHz) continuous wave (CW) EPR spectrum of as-isolated CPSF73 at 10 K reveals three distinct signals (Fig. 4).

1) An axial signal centered at approximately 370 mT with *g*-values of $g_{\perp} = 1.92$ and $g_{\parallel} = 1.78$ which can be assigned to an Fe(II)-Fe(III) diiron complex in which antiferromagnetic coupling between the $S = 2$ Fe(II) and $S = 5/2$ Fe(III) ions produces an effective $S = 1/2$ ground state. This EPR signal is similar to that observed for diiron centers in the Type I Cas3 nucleases when reduced with ascorbate ($g_{\perp} = 1.93$, $g_{\parallel} = 1.78$) (29). Quantitation of this signal by comparison to a 300 μM $CuSO_4$ spin standard sample indicates that this signal corresponds to 10 μM or approximately 4% of the CPSF73 within the sample. Addition of sodium ascorbate in 10-fold excess as a chemical reductant did not change the intensity of this signal.
2) A relatively broad isotropic signal centered at 160 mT ($g = 4.29$) which can be assigned to high-spin ($S = 5/2$) mononuclear Fe(III) with a fully rhombic (E/D ≈ 0.33) zero-field

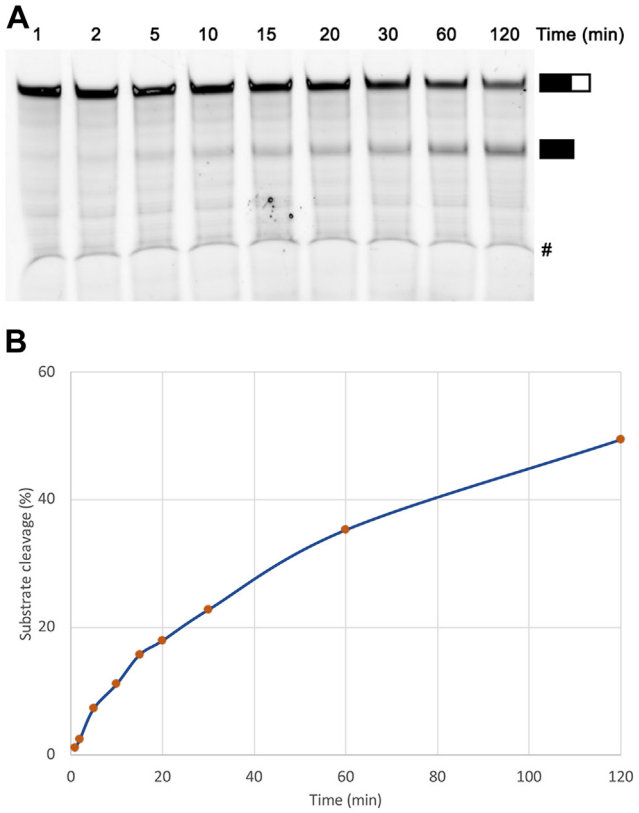

Figure 3. Endonuclease cleavage of a model pre-mRNA substrate by a reconstituted canonical machinery. *A*, a time course of the cleavage reaction, using the same 70-mer pre-mRNA substrate. The protein factors were expressed in insect cells and indicated with #. *B*, the reaction time course converted to percentage of substrate cleavage, based on the intensity of the substrate and product bands.

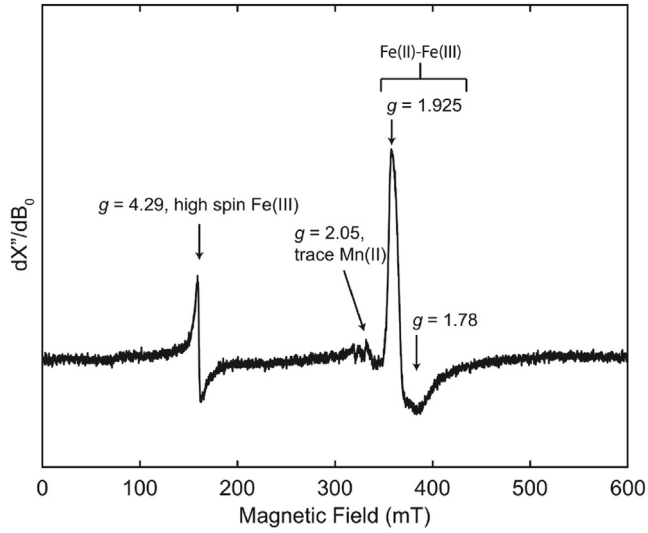

Figure 4. X-band CW-EPR spectrum of CPSF73 catalytic segment acquired at a temperature of 10 K with effective g-values and identities of relevant signals denoted. Acquisition parameters: microwave frequency = 9.637 GHz, modulation amplitude = 0.8 mT, modulation frequency = 100 KHz, conversion time = 10 ms. CPSF, cleavage and polyadenylation specificity factor; CW, continuous wave; EPR, electron paramagnetic resonance.

splitting interaction between the five unpaired Fe d-electrons—indicative of approximately tetrahedral (or lower) coordination symmetry. This may arise from Fe(III) in the bimetallic site paired with a diamagnetic metal (Zn), or adventitiously bound or free Fe(III) in the sample buffer.

3) An extremely low-intensity signal at the low field edge of the Fe(II)-Fe(III) dimer signal centered at approximately g = 2.05. This very likely corresponds to a small amount of Mn(II) which, though high spin (S = 5/2), when in high symmetry octahedral coordination environments such as $Mn(II)(H_2O)_6$, exhibits very small zero-field splitting, and typically is centered at g = 2.05. The fine structure of this signal is due to the hyperfine interaction with the 100% abundant I = 5/2 ^{55}Mn nucleus, which produces a 6-line splitting of ∼ 8.8 mT. Only three of these Mn hyperfine peaks are resolved here, due to overlap with the Fe(II)-Fe(III) signal.

Altogether, the EPR spectroscopy indicates and corroborates the presence of Fe in both Fe(II) and Fe(III) oxidation states, as well as trace amounts of Mn(II). It should be noted that if the majority of the bimetallic cofactor is comprised of diiron metalation and the metals are antiferromagnetically coupled, the Fe(II)-Fe(II) and Fe(III)-Fe(III) oxidation states will both be diamagnetic and thus EPR-silent. This may explain the 4% abundance of Fe(II)-Fe(III) observed by EPR spectroscopy.

Metal ions in INTS11 active site

Our data on the metal ions in the active site of CPSF73 prompted us to examine the metal ions in the active site of its homolog INTS11. We subjected a sample of human ICM expressed in insect cells to ICP-MS and found that Mn is the most abundant, at 41%, followed by Fe (31%) and Zn (26%) (Table 1). Therefore, the active site of INTS11 also contains a mixture of metal ions in this sample.

Discussion

Metallo-β-lactamases comprise a large family of enzymes and have been identified from a wide variety of living organisms (30–32). Their active sites can have 1 or 2 metal ions, and structural studies with CPSF73 and its homolog INTS11 demonstrate that they have two metal ions in the active site, with each metal ion octahedrally coordinated by strictly conserved residues from the enzyme, the scissile phosphate of the RNA substrate, and a water/hydroxide (Fig. 1*B*). Most metallo-β-lactamases use zinc as the metal ion for their catalysis, and it has been thought that CPSF73 also uses zinc for its catalysis. Prior experimental evidence for zinc in the active site of CPSF73 includes the observation that N,N,N′,N′-tetrakis(2-pyridylmethyl)ethylenediamine and ortho-phenanthroline can inhibit the cleavage activity of nuclear extracts (7). However, these compounds are not zinc specific, and they can also chelate other heavy metals, such as Fe and Mn. Therefore, the inhibitory activity of these compounds cannot rule out the presence of other metal ions in the active site of CPSF73.

Our studies have shown that recombinant CPSF73, expressed in *E. coli*, insect, or human cells, contains a substantial amount of iron as the metal ion in the active site, and the samples purified from insect and human cells possess nuclease activity toward pre-mRNA substrates. While our data do not directly demonstrate whether CPSF73 with iron in the active site is active at RNA cleavage, the good activity that we observed in our cleavage assays with the sample from insect cells and the high abundance of iron in CPSF73 in that sample are strongly consistent with the hypothesis that iron can support the catalytic activity of CPSF73, which is further supported by the observation of the comparable activity for CPSF73 expressed in human cells, even though it has much higher zinc content. If CPSF73 is active only with two zinc ions in the active site, only ∼3% of the sample from insect cells would be active (0.18 × 0.18), assuming the metal ions are distributed randomly between the two sites. In comparison, ∼56% of the sample from human cells would be active (0.75 × 0.75), but its activity is generally comparable to what we observed with the sample from insect cells (Fig. S2), while a ∼20-fold difference in activity would have been expected.

There is precedence for Fe, Mn, or other transition metal ions being active catalytically in metallo-β-lactamases (23–25). Plant glyoxalase II may be an especially good case for comparison with CPSF73 and INTS11. The protein ligands of the two metal ions in the active site of glyoxalase II are identical to those in CPSF73 and they, as well as a bridging water/hydroxide, are arranged equivalently also (33) (Fig. S3, *A* and *B*). EPR spectroscopy studies indicate the presence of Fe(III)-Zn(II), Fe(III)-Fe(II) and other metal ion combinations in the active site of mitochondrial glyoxalase II, Fe(III)-Zn(II), Fe(III)-Fe(II), and Mn(II)-Mn(II) metal centers in cytoplasmic glyoxalase II, and these samples are active for hydrolyzing substrates (33–35). Therefore, our observations with CPSF73 are similar to those with glyoxalase II, offering further support to the idea that CPSF73 can use metal ions other than zinc for catalysis. It is also worth noting that, like these other metallo-β-lactamases, CPSF73 is a hydrolase and is not expected to undergo oxidation-reduction during the nuclease reaction. Therefore, both Fe(III) and Fe(II) could support the catalytic activity, as seen with glyoxalase II, with their role being to coordinate the scissile phosphate of the substrate and activating the water/hydroxide nucleophile (Fig. 1*B*).

To definitively prove whether metal ions other than Zn can support catalysis by CPSF73, we would need to obtain an mCF/HCC sample that is fully loaded with zinc or iron for nuclease assays. However, our experiments at supplementing the reaction buffer with extra Zn(II), Fe(II), and Fe(III) did not lead to any changes in the cleavage activity (Fig. S1). The inclusion of Zn in the crystallization buffer did not replace the Fe in the active site of CPSF73 catalytic segment. EDTA cannot remove the metal ions bound in the active site of CPSF73 either. Therefore, changing the metal ion composition of CPSF73 in mCF/HCC would require unfolding the three mCF subunits (or four for HCC) to release the metal ions in CPSF73 and refolding them in the presence of the desired metal ion, which is very challenging technically.

Studies with other metallo-β-lactamases suggest that metal loading in the active site depends on the concentration of metal ions in the media (24). We purified CPSF73 from expression in three different sources (bacteria, insect, and human cells) and found three different metal ion contents, consistent with a role for the expression media and expression host. However, the concentration of Fe (∼μM) in the cytosol in human cells is much higher than that of Zn (∼0.2 μM) (36), although zinc was found to be the more abundant metal in HCC expressed in human cells (Table 1). We supplemented bacterial growth media with 0.1 mM zinc during the structure determination of the CPSF73 catalytic segment, but the two metal ions in the active site are still mostly iron (9). The concentrations of various free metal ions in the cell are likely maintained at low levels, as high concentrations are toxic (36). The loading of metal ions into the active site of metallo-β-lactamases may also be regulated (37). A zinc metallochaperone was recently identified for the zinc metalloprotease methionine aminopeptidase 1 (38, 39). The mechanism how metal ions are delivered and incorporated into the active sites of CPSF73 and INTS11 is currently not known. The different metal ion content of CPSF73 from the different expression hosts (Table 1) also suggests the possibility that endogenous CPSF73 could have different metal contents in different organisms.

Many nucleases use Mg^{2+} or Mn^{2+} as the metal ion for catalysis, with one, two, or three of the metal ions in the active site (40). Some examples include RNase H (41), Argonaute (42), dicer, restriction endonucleases, 5′ exoribonucleases, and the decapping exonuclease DXO and related enzyme Rai1 (43, 44). As is the case with CPSF73 and INTS11, the metal ions coordinate the scissile phosphate of the substrate and possibly also activate the nucleophile for the hydrolysis reaction. On the other hand, there are also many examples of nucleases that use zinc and other transition metal ions for catalysis besides CPSF73 and INTS11, such as AP endonuclease IV (40). Type I Cas3 nuclease is another good example, which is active with Fe, Co, Mn, and Ni homodimetal centers, with Fe(II)-Fe(II) being the most active (29). The two metal ions are coordinated octahedrally by 5 His and 2 Asp residues (45), bearing substantial similarity to the active sites of CPSF73 and INTS11.

Our studies have revealed that a mixture of transition metal ions exists in the active site of CPSF73 and that metal ions other than zinc may be able to support its nuclease activity. We have found that human INTS11 also contains a mixture of metal ions in its active site. It would be interesting to examine the metal ion content in the active site of related metallo-β-lactamase enzymes involved in RNA metabolism, for example RNase J and RNase Z (46–49), and possibly metallo-β-lactamases in general.

Experimental procedures

Protein expression and purification

The catalytic segment of human CPSF73 was expressed in *E. coli* and purified following protocols described earlier (9). The N-terminal 6 × His-tagged CPSF73 (residues 1–460) was

overexpressed in *E. coli* BL21 (DE3) Rosetta cells at 18 °C overnight. Harvested cell pellets were resuspended in lysis buffer containing 20 mM Tris (pH 8.0), 300 mM NaCl, 20 mM imidazole, 10 mM β-mercaptoethanol, and 1 × phenylmethylsulfonyl fluoride. The resuspended cells were lysed through sonication, followed by centrifugation at 12,000 rpm and 4 °C to remove debris. The cell-free lysate was incubated with pre-equilibrated Ni-NTA beads (Qiagen) for 1 h at 4 °C. The beads were washed at least 5 column volumes before eluting the target protein with 20 mM Tris (pH 8.0), 300 mM NaCl, 250 mM imidazole, and 10 mM β-mercaptoethanol. Fractions containing CPSF73 were pooled and injected onto a pre-equilibrated gel filtration column (HiLoad 16/60 Superdex 200 prep grade, Cytiva) with the running buffer 20 mM Tris (pH 8.0), 250 mM NaCl, and 5 mM DTT. The purified protein was concentrated, flash frozen in liquid nitrogen, and stored at −80 °C.

The recombinant protein samples for nuclease assays were expressed in insect cells unless otherwise noted. For mPSF, our earlier samples combined components that were expressed separately or on different vectors (50, 51). For the studies here, full-length human CPSF160, CPSF30, and Fip1 were inserted into the 438A vector (Addgene #55218) and WDR33 (1–572) was inserted into the 438C vector (Addgene #55220, which adds an N-terminal 6 × His-MBP tag followed by a TEV cleavage site) using Gibson assembly (NEB E2611L) (52). All four subunits were combined into one vector by three rounds of Gibson assembly.

For mCF, two sets of expression constructs were used. Both included full-length CPSF73 and CPSF100. One lacked the NTD of symplekin (containing residues 538–1110), as described earlier (51). The other contained the NTD (residues 30–1101) as well as CstF64 and is therefore the HCC (15, 18). Both are active in the cleavage assays, confirming that the symplekin NTD is not required for the activity of the canonical machinery (14) while it is essential for histone pre-mRNA 3′-end processing (18, 26).

For CstF, full-length CstF64 and CstF50 were inserted into the 438A vector and CstF77 was inserted into the 438C vector using Gibson assembly, and the three subunits were combined into one vector by two rounds of Gibson assembly.

For CFIIm, Pcf11 (full-length, 770–1555, or 1195–1555) (28) and full-length Clp1 were inserted into the pFL vector (53) with an N-terminal 6×His tag on Pcf11. RBBP6 (1–399) was inserted into the pFL vector with an N-terminal 6×His tag. Full-length PAP was inserted into the pFL vector with an N-terminal 6×His tag, and the D115A catalytically dead mutant was generated by site-directed mutagenesis PCR. This mutant can support the cleavage activity in the reconstituted canonical machinery (13). For CFIm, CFIm68 and CFIm25 were inserted into the pFL vector with an N-terminal 6×His tag on CFIm25.

All proteins were expressed in Tni insect cells (Expression Systems) and purified following protocols described earlier (51), except that CstF and mPSF were further purified by amylose resin before the Superose 6 10/300 Gl column (Cytiva).

A sample of human HCC was also expressed in human cells for ICP-MS analysis. HEK293T stable expression cell lines were established as described before (13). Briefly, pools of cells that stably expressed HCC (TwinStrep-3C-Symplekin, CPSF100, CPSF73, CstF64) were generated using the *piggybac* transposon system by initially transfecting the cells using polyethyleneimine (54, 55). For protein expression, cultures were adjusted to a density of 1×10^6 cells per ml in FreeStyle 293 expression medium (Gibco, Thermo Fisher Scientific). The cells were induced with doxycycline and harvested 48 h after induction. Pellets were lysed with a glass dounce homogenizer in buffer containing 1× Dulbecco's phosphate buffered saline, 2 mM DTT supplemented for lysis with EDTA-free cOmplete protease inhibitor cocktail (Roche), DNase I and benzonase. After clearing the lysate by centrifugation, HCC was purified using a StrepTrap HP column (Cytiva). After washing with lysis buffer and lysis buffer supplemented to 300 mM NaCl, bound proteins were eluted with 5 mM desthiobiotin in lysis buffer. The elution fractions were concentrated and further purified over a Superose 6i 10/300 gel filtration column (Cytiva) in 20 mM Hepes (pH 7.9), 150 mM NaCl, and 2 mM DTT. Fractions containing pure protein were pooled, concentrated and flash frozen in liquid nitrogen.

RNA cleavage assays

The model RNA substrate contains 70 nucleotides (nts), with a 5′ FAM label, and encompasses the SV40 late mRNA 3′-end processing site. The sequence of the RNA is CUUUA UUUGUAACCAUUAUAAGCUGCAAUAAACAAGUUAAC AACA|ACAAUUGCAUUCAUUUUAUGUUUCA, where the AAUAAA poly(A) signal is underlined, and the cleavage site is indicated with the vertical bar. The cleavage products include a 45 nts 5′ fragment (with 5′ FAM label) and a 25 nts 3′ fragment (no label). The RNA substrate is included in the cleavage reaction at 125 nM concentration.

For the pre-mRNA cleavage assays with the HeLa cell nuclear extract supplemented with recombinant proteins, the nuclear extract was obtained from a commercial source (Ipracell) (28). 10% (v/v) 2 M KCl was added to the extract and the mixture centrifuged at 13,000 rpm for 10 min to remove any insoluble material. Various recombinant proteins were included in the assay as indicated. The reaction buffer contained 20 mM Hepes (pH 8.0), 75 mM KCl, 4 mM DTT, 2.5% (w/v) PEG6000, 20 mM CP, 2.5 mM ATP, 2 mM EDTA, and RNase inhibitor. The reaction mixture was incubated at 30 °C for 2 h. The reaction products were separated by gel electrophoresis and imaged with a Chem-iDoc system (Bio-Rad). For the time course, various time points were taken, and the intensity of the bands was determined with ImageJ (56).

For the pre-mRNA cleavage assays with the reconstituted canonical machinery, the reaction contained purified mPSF, mCF (or HCC), CstF, CFIIm, and PAP (D115A) at 0.25 μM concentration and RBBP6 (1–399) at 1 μM concentration. The reaction buffer contained 20 mM Hepes (pH 7.5), 75 mM KCl,

4 mM DTT, 2.5% (w/v) PEG6000, 2 mM Mg^{2+} acetate, 2.5 mM ATP, and 10 μM $ZnCl_2$. The mixture was incubated at 30 °C, and various time points were taken for the time course.

ICP-MS experiments

The ICP-MS experiments on bacterially expressed human CPSF73 catalytic segment were carried out at the University of Missouri, Columbia, in 2007. Approximately, 50 μl of the protein sample at 0.1 mM concentration was placed in a precleaned polypropylene centrifuge tube for digestion with nitric acid (Fisher Scientific, Optima grade) and 30% hydrogen peroxide (Fluka, TraceSelect grade). The tube was sealed and heated for 1 h in an ultrasonic bath maintained at 60 °C. The digested solution was diluted to 10 ml, and then the internal standards Be, Y, and Cd were added. The solution thus prepared was analyzed by high-resolution ICP-MS. The VG Axiom high-resolution ICP-MS was calibrated using two linearity standards prepared from a commercial high-purity multielement standards solution. The internal standards were added to the calibration standards at the same level as in the sample solution. The sample limit of detection was calculated by multiplying the instrument limit of detection by the total sample dilution factor.

The ICP-MS experiments on recombinant human mCF expressed in insect cells, human HCC expressed in human cells, and human ICM expressed in insect cells were carried out at Columbia University. The sample (120 μl at 40 μM concentration) was transferred to 15 ml metal-free tubes (Labcon), and 200 μl concentrated nitric acid (Optima, Fisher Scientific, ultra-trace 67–70%) was added, and the sample was digested overnight at room temperature. An internal standard was then added to the digest (20 μl of a solution containing 500 μg/l Ga in 2% (v/v) HNO_3), and the mixture diluted to 2 ml with an aqueous solution (20× dilution). The sample was diluted in a second step (final dilution 200×) and measured on ICP-MS (NexION 350s): Mn and Fe (Ammonia mode), Ni and Zn (no gas mode). The relative standard deviations for measured Mn (n = 7), Fe (n = 7), Ni (n = 7), and Zn (n = 6) are 4, 6, 3, and 9%, respectively, for the human mCF sample, 8%, 6%, 8%, and 9% (all n = 6), respectively, for the human HCC sample, and 1%, 1%, 0.3%, and 4% (all n = 6), respectively, for the human ICM sample.

EPR spectroscopy

X-band (9.6 GHz) CW EPR spectra were acquired using a Bruker EMX CW-EPR spectrometer equipped with an ER-4116DM Dual Mode resonator operating in perpendicular mode. Temperature control was achieved through use of an Oxford Instruments ESR-900 liquid helium flow cryostat and an ITC-503 temperature controller.

X-ray diffraction data collection and processing

Crystals of human CPSF73 catalytic segment were produced following protocols described earlier (9), without any zinc in the crystallization solution, and frozen in liquid nitrogen. X-ray diffraction datasets were collected at 100K at the NE-CAT 24-ID-C beamline at the Advanced Photon Source, at the Mn, Fe and Zn absorption peak. The diffraction patterns were recorded with a Dectris EIGER2 16M detector, and the images were processed with XDS (57). The data processing statistics are summarized in Table S1. Anomalous data between 15 and 3 Å resolution were used to calculate anomalous difference electron density maps with CCP4 (58), using phase information from the atomic model. The map contained 180, 240, and 320 grid points along the *a*, *b*, and *c* axes, respectively, to ensure sufficient sampling of the peaks. The top peaks in the difference map were identified.

Data availability

The data underlying this article will be shared on reasonable request to the corresponding author.

Supporting information—This article contains supporting information.

Acknowledgments

We thank James Guthrie, University of Missouri, for carrying out the ICP-MS analysis on the CPSF73 catalytic segment in 2007 and Kathrin Schilling, Columbia University Mailman School of Public Health, for carrying out the ICP-MS analysis on mCF, HCC and ICM.

Author contributions—J. H., X. L., Y. S., Z. L., M.-H. L., K. H., C. R. M., E. C., P. H. O., L. T., and F. S. conceptualization; J. H., X. L., Y. S., Z. L., K. H., M.-H. L., P. H. O., F. S., E. C., L. T., and C. R. M. investigation; P. H. O. and L. T. formal analysis; J. H., X. L., Y. S., Z. L., M.-H. L., K. H., C. R. M., F. S., E. C., P. H. O., and L. T. methodology; L. T., E. C., and P. H. O. supervision; J. H., X. L., Y. S., Z. L., M.-H. L., K. H., C. R. M., E. C., P. H. O. L. T., and F. S. visualization; E. C., P. H. O., and L. T. funding acquisition; L. T., P. H. O., J. H., X. L., and F. S. writing-original draft.

Funding and additional information—This research is supported by NIH grant R35GM118093 (to L. T.). This work is based in part on research conducted at the Northeastern Collaborative Access Team beamlines, which are funded by the National Institute of General Medical Sciences from the National Institutes of Health (P30 GM124165). This research used resources of the Advanced Photon Source, a U.S. Department of Energy (DOE), Office of Science User Facility operated for the DOE Office of Science by Argonne National Laboratory under Contract No. DE-AC02-06CH11357. The content is solely the responsibility of the authors and does not necessarily represent the official views of the National Institutes of Health. The Caltech EPR facility acknowledges support from the Beckman Institute and the Dow Next Generation Educator Fund.

Conflict of interest—The authors declare that they have no conflicts of interest with the contents of this article.

Abbreviations—The abbreviations used are: CstF, cleavage stimulation factor; CFIm, cleavage factor Im; CPSF, cleavage and polyadenylation specificity factor; CW, continuous wave; EPR, electron paramagnetic resonance; HCC, histone pre-mRNA cleavage complex; ICP-MS, inductively coupled plasma mass spectrometry; ICM, Integrator cleavage module; mCF, mammalian cleavage factor;

mPSF, mammalian polyadenylation specificity factor; PAP, poly(A) polymerase; PEG, polyethylene glycol.

References

1. Zhao, J., Hyman, L., and Moore, C. L. (1999) Formation of mRNA 3′ ends in eukaryotes: mechanism, regulation, and interrelationships with other steps in mRNA synthesis. *Microbiol. Mol. Biol. Rev.* **63**, 405–445
2. Proudfoot, N. J. (2011) Ending the message: poly(A) signals then and now. *Genes Develop.* **25**, 1770–1782
3. Yang, Q., and Doublie, S. (2011) Structural biology of poly(A) site definition. *Wiley Interdiscip. Rev. RNA* **2**, 732–747
4. Shi, Y., and Manley, J. L. (2015) The end of the message: multiple protein-RNA interactions define the mRNA polyadenylation site. *Genes Develop.* **29**, 889–897
5. Sun, Y., Hamilton, K., and Tong, L. (2020) Recent molecular insights into canonical pre-mRNA 3′-end processing. *Transcription* **11**, 83–96
6. Dominski, Z., and Marzluff, W. F. (2007) Formation of the 3′ end of histone mRNA: getting closer to the end. *Gene* **396**, 373–390
7. Ryan, K., Calvo, O., and Manley, J. L. (2004) Evidence that polyadenylation factor CPSF-73 is the mRNA 3′ processing endonuclease. *RNA* **10**, 565–573
8. Dominski, Z., Yang, X.-C., and Marzluff, W. F. (2005) The polyadenylation factor CPSF-73 is involved in histone-pre-mRNA processing. *Cell* **123**, 37–48
9. Mandel, C. R., Kaneko, S., Zhang, H., Gebauer, D., Vethantham, V., Manley, J. L., *et al.* (2006) Polyadenylation factor CPSF-73 is the pre-mRNA 3′-end-processing endonuclease. *Nature* **444**, 953–956
10. Chan, S. L., Huppertz, I., Yao, C., Weng, L., Moresco, J. J., Yates, J. R., III, *et al.* (2014) CPSF30 and Wdr33 directly bind to AAUAAA in mammalian mRNA 3′ processing. *Genes Develop.* **28**, 2370–2380
11. Schonemann, L., Kuhn, U., Martin, G., Schafer, P., Gruber, A. R., Keller, W., *et al.* (2014) Reconstitution of CPSF active in polyadenylation: recognition of the polyadenylation signal by WDR33. *Genes Develop.* **28**, 2381–2393
12. Shi, Y., di Giammartino, D. C., Taylor, D., Sarkeshik, A., Rice, W. J., Yates, J. R., III, *et al.* (2009) Molecular architecture of the human pre-mRNA 3′ processing complex. *Mol. Cell* **33**, 365–376
13. Schmidt, M., Kluge, F., Sandmeir, F., Kühn, U., Schäfer, P., Tüting, C., *et al.* (2022) Reconstitution of 3′ end processing of mammalian pre-mRNA reveals a central role of RBBP6. *Genes Dev.* **36**, 195–209
14. Boreikaite, V., Elliott, T. S., Chin, J. W., and Passmore, L. A. (2022) RBBP6 activates the pre-mRNA 3′ end processing machinery in humans. *Genes Dev.* **36**, 210–224
15. Yang, X.-C., Sabath, I., Debski, J., Kaus-Drobek, M., Dadlez, M., Marzluff, W. F., *et al.* (2013) A complex containing the CPSF73 endonuclease and other poyadenylation factors associates with U7 snRNP and is recruited to histone pre-mRNA for 3′-end processing. *Mol. Cell. Biol.* **33**, 28–37
16. Callebaut, I., Moshous, D., Mornon, J.-P., and de Villartay, J.-P. (2002) Metallo-b-lactamase fold within nucleic acids processing enzymes: The b-CASP family. *Nucl. Acid Res.* **30**, 3592–3601
17. Dominski, Z., Carpousis, A. J., and Clouet-d'Orval, B. (2013) Emergence of the b-CASP ribonucleases: highly conserved and ubiquitous metallo-enzymes involved in messenger RNA maturation and degradation. *Biochim. Biophys. Acta* **1829**, 532–551
18. Sun, Y., Zhang, Y., Aik, W. S., Yang, X. C., Marzluff, W. F., Walz, T., *et al.* (2020) Structure of an active human histone pre-mRNA 3′-end processing machinery. *Science* **367**, 700–703
19. Baillat, D., Hakimi, M.-A., Naar, A. M., Shilatifard, A., Cooch, N., and Shiekhattar, R. (2005) Integrator, a multiprotein mediator of small nuclear RNA processing, associates with the C-terminal repeat of RNA polymerase II. *Cell* **123**, 265–276
20. Mendoza-Figueroa, M. S., Tatomer, D. C., and Wilusz, J. E. (2020) The integrator complex in transcription and development. *Trends Biochem. Sci.* **45**, 923–934
21. Kirstein, N., Gomes Dos Santos, H., Blumenthal, E., and Shiekhattar, R. (2020) The Integrator complex at the crossroad of coding and noncoding RNA. *Curr. Opin. Cell Biol.* **70**, 37–43
22. Wagner, E. J., Tong, L., and Adelman, K. (2023) Integrator is a global promoter-proximal termination complex. *Mol. Cell* **83**, 416–427
23. Badarau, A., and Page, M. I. (2006) The variation of catalytic efficiency of Bacillus cereus metallo-beta-lactamase with different active site metal ions. *Biochemistry* **45**, 10654–10666
24. Hu, Z., Gunasekera, T. S., Spadafora, L., Bennett, B., and Crowder, M. W. (2008) Metal content of metallo-beta-lactamase L1 is determined by the bioavailability of metal ions. *Biochemistry* **47**, 7947–7953
25. Carruthers, T. J., Carr, P. D., Loh, C. T., Jackson, C. J., and Otting, G. (2014) Iron(III) located in the dinuclear metallo-β-lactamase IMP-1 by pseudocontact shifts. *Angew. Chem. Int. Ed. Engl.* **53**, 14269–14272
26. Yang, X. C., Sun, Y., Aik, W. S., Marzluff, W. F., Tong, L., and Dominski, Z. (2020) Studies with recombinant U7 snRNP demonstrate that CPSF73 is both an endonuclease and a 5′-3′ exonuclease. *RNA* **26**, 1345–1359
27. Sun, Y., Aik, W. S., Yang, X.-C., Marzluff, W. F., Dominski, Z., and Tong, L. (2021) Reconstitution and biochemical assays of an active human histone pre-mRNA 3′-end processing machinery. *Methods Enzymol.* **655**, 291–324
28. Schafer, P., Tuting, C., Schonemann, L., Kuhn, U., Treiber, T., Treiber, N., *et al.* (2018) Reconstitution of mammalian cleavage factor II involved in 3′ processing of mRNA precursors. *RNA* **24**, 1721–1737
29. Sun, S., He, Z., Jiang, P., Baral, R., and Pandelia, M. E. (2022) Metal dependence and functional diversity of Type I Cas3 nucleases. *Biochemistry* **61**, 327–338
30. Ju, L. C., Cheng, Z., Fast, W., Bonomo, R. A., and Crowder, M. W. (2018) The continuing challenge of metallo-β-lactamase inhibition: mechanism matters. *Trends Pharmacol. Sci.* **39**, 635–647
31. Boyd, S. E., Livermore, D. M., Hooper, D. C., and Hope, W. W. (2020) Metallo-β-Lactamases: structure, function, epidemiology, treatment options, and the development pipeline. *Antimicrob. Agents Chemother.* **64**, e00397-20
32. Bahr, G., González, L. J., and Vila, A. J. (2021) Metallo-β-lactamases in the age of multidrug resistance: from structure and mechanism to evolution, dissemination, and inhibitor design. *Chem. Rev.* **121**, 7957–8094
33. Marasinghe, G. P., Sander, I. M., Bennett, B., Periyannan, G., Yang, K. W., Makaroff, C. A., *et al.* (2005) Structural studies on a mitochondrial glyoxalase II. *J. Biol. Chem.* **280**, 40668–40675
34. Schilling, O., Wenzel, N., Naylor, M., Vogel, A., Crowder, M., Makaroff, C., *et al.* (2003) Flexible metal binding of the metallo-beta-lactamase domain: Glyoxalase II incorporates iron, manganese, and zinc *in vivo*. *Biochemistry* **42**, 11777–11786
35. Wenzel, N. F., Carenbauer, A. L., Pfiester, M. P., Schilling, O., Meyer-Klaucke, W., Makaroff, C. A., *et al.* (2004) The binding of iron and zinc to glyoxalase II occurs exclusively as di-metal centers and is unique within the metallo-beta-lactamase family. *J. Biol. Inorg. Chem.* **9**, 429–438
36. Bischof, H., Burgstaller, S., Waldeck-Weiermair, M., Rauter, T., Schinagl, M., Ramadani-Muja, J., *et al.* (2019) Live-cell imaging of physiologically relevant metal ions using genetically encoded FRET-based probes. *Cells* **8**, 492
37. Bahr, G., González, L. J., and Vila, A. J. (2022) Metallo-β-lactamases and a tug-of-war for the available zinc at the host-pathogen interface. *Curr. Opin. Chem. Biol.* **66**, 102103
38. Weiss, A., Murdoch, C. C., Edmonds, K. A., Jordan, M. R., Monteith, A. J., Perera, Y. R., *et al.* (2022) Zn-regulated GTPase metalloprotein activator 1 modulates vertebrate zinc homeostasis. *Cell* **185**, 2148–2163.e27
39. Pasquini, M., Grosjean, N., Hixson, K. K., Nicora, C. D., Yee, E. F., Lipton, M., *et al.* (2022) Zng1 is a GTP-dependent zinc transferase needed for activation of methionine aminopeptidase. *Cell Rep.* **39**, 110834
40. Yang, W. (2011) Nucleases: diversity of structure, function and mechanism. *Quart. Rev. Biophys.* **44**, 1–93
41. Nowotny, M., and Yang, W. (2006) Stepwise analyses of metal ions in RNase H catalysis from substrate destabilization to product release. *EMBO J* **25**, 1924–1933

42. Wang, Y., Juranek, S., Li, H., Sheng, G., Wardle, G. S., Tuschl, T., *et al.* (2009) Nucleation, propagation and cleavage of target RNAs in Ago silencing complexes. *Nature* **461**, 754–761
43. Jiao, X., Chang, J. H., Kilic, T., Tong, L., and Kiledjian, M. (2013) A mammalian pre-mRNA 5′ end capping quality control mechanism and an unexpected link of capping to pre-mRNA processing. *Mol. Cell* **50**, 104–115
44. Wang, V. Y., Jiao, X., Kiledjian, M., and Tong, L. (2015) Structural and biochemical studies of the distinct activity profiles of Rai1 enzymes. *Nucl. Acid Res.* **43**, 6596–6606
45. Huo, Y., Nam, K. H., Ding, F., Lee, H., Wu, L., Xiao, Y., *et al.* (2014) Structures of CRISPR Cas3 offer mechanistic insights into Cascade-activated DNA unwinding and degradation. *Nat. Struct. Mol. Biol.* **21**, 771–777
46. de la Sierra-Gallay, I. L., Zig, L., Jamalli, A., and Putzer, H. (2008) Structural insights into the dual activity of RNase J. *Nat. Struct. Mol. Biol.* **15**, 206–212
47. de la Sierra-Gallay, I. L., Pellegrini, O., and Condon, C. (2005) Structural basis for substrate binding, cleavage and allostery in the tRNA maturase RNase Z. *Nature* **433**, 657–661
48. Ishii, R., Minagawa, A., Takaku, H., Takagi, M., Nashimoto, M., and Yokoyama, S. (2005) Crystal structure of the tRNA 3′ processing endoribonuclease tRNase Z from Thermotoga maritima. *J. Biol. Chem.* **280**, 14138–14144
49. Bechhofer, D. H., and Deutscher, M. P. (2019) Bacterial ribonucleases and their roles in RNA metabolism. *Crit. Rev. Biochem. Mol. Biol.* **54**, 242–300
50. Sun, Y., Zhang, Y., Hamilton, K., Manley, J. L., Shi, Y., Walz, T., *et al.* (2018) Molecular basis for the recognition of the human AAUAAA polyadenylation signal. *Proc. Natl. Acad. Sci. U. S. A.* **115**, E1419–E1428
51. Zhang, Y., Sun, Y., Shi, Y., Walz, T., and Tong, L. (2020) Structural insights into the human pre-mRNA 3′-end processing machinery. *Mol. Cell* **77**, 800–809
52. Gibson, D. G., Young, L., Chuang, R. Y., Venter, J. C., Hutchison, C. A., 3rd, and Smith, H. O. (2009) Enzymatic assembly of DNA molecules up to several hundred kilobases. *Nat. Methods* **6**, 343–345
53. Sari, D., Gupta, K., Thimiri Govinda Raj, D. B., Aubert, A., Drncova, P., Garzoni, F., *et al.* (2016) The MultiBac baculovirus/insect cell expression vector system for producing complex protein biologics. *Adv. Exp. Med. Biol.* **896**, 199–215
54. Yusa, K., Zhou, L., Li, M. A., Bradley, A., and Craig, N. L. (2011) A hyperactive piggyBac transposase for mammalian applications. *Proc. Natl. Acad. Sci. U. S. A.* **108**, 1531–1536
55. Li, X., Burnight, E. R., Cooney, A. L., Malani, N., Brady, T., Sander, J. D., *et al.* (2013) piggyBac transposase tools for genome engineering. *Proc. Natl. Acad. Sci. U. S. A.* **110**, E2279–2287
56. Schneider, C. A., Rasband, W. S., and Eliceiri, K. W. (2012) NIH image to ImageJ: 25 years of image analysis. *Nat. Methods* **9**, 671–675
57. Kabsch, W. (2010) Integration, scaling, space-group assignment and post-refinement. *Acta Cryst.* **D66**, 133–144
58. CCP4. (1994) The CCP4 suite: programs for protein crystallography. *Acta Cryst.* **D50**, 760–763